SCIENTIFIC REPORTS

natureresearch

Check for updates

OPEN

Extraction technique of trap states based on transient photo-voltage measurement

Zedong Lin

This article puts forward a technique for extracting the density of trap states (DOS$_T$) distribution based on the transient photo-voltage (TPV) measurement result. We prove that when the TPV result is linear, the DOS$_T$ distribution is exponential type and vice versa. Compared to the approach based on the space charge limited current measurement, the method given in this paper has the advantage of requiring less calculation. The results obtained by our method provides a guidance for preparing less trap states solar cells.

In order to improve the photo-voltaic performance of perovskite solar cells (PSCs), we need to further explore the mechanism such as carrier mobility[1–3], ion migration[4–8], density of trap states (DOS$_T$) distribution[9–13], carrier recombination[14–18] and so on. The DOS$_T$ distribution is a crucial factor that determines the photovoltaic performance of PSCs[19–33]. According to the literatures in recent years[19–23], current density–voltage (J–V) hysteresis is caused by the ion migration and trap assisted carrier recombination. The DOS$_T$ distribution affects the carrier recombination[24–27], influences the open circuit voltage[28–30], and hinders the enhancement of power conversion efficiency (PCE)[31–34]. The DOS$_T$ distribution cannot be obtained by experimental measurement directly. There are only few methods for the extraction of DOS$_T$ distribution. The space charge limited current (SCLC) method uses the deconvolution to extract the DOS$_T$ distribution[35–40], based on the measured J–V data at different temperatures. Walter et al.[41–45] put forward the impedance spectroscopy (IS) method to extract the DOS$_T$ distribution. They extract the DOS$_T$ distribution based on the plot of equivalent chemical capacitance versus frequency given by IS measurement[41–45]. They regard the capture and de-capture of carrier by the trap states in the PSCs as charging and discharging of the equivalent chemical capacitance[41]. They put forward the formula $DOS_T (E_\omega) = (V_{bi}/eW)(dC/d\omega)(\omega/k_B)$ to extract the DOS$_T$ distribution[41–45]. Here, C is the equivalent chemical capacitance. ω is the angular frequency of the ac signal. V_{bi} is the built-in electric voltage. W is the depletion width. k_B is the Boltzmann constant. e is the elementary charge. The corresponding energy level is calculated by the formula $E_\omega = k_B T \ln(\omega_0/\omega)$, where T is the ambient temperature and ω_0 is the attempt-to-escape frequency[41–45]. Wang et al.[46] proposed a transient photo-voltage (TPV) method for DOS$_T$ distribution extraction. Based on the hypothesis of exponential type DOS$_T$ distribution[46–49], multiple-trapping model[46,50–52], and the zero-temperature approximation[46,52], they find that when the DOS$_T$ distribution is exponential type, the logarithm of carrier lifetime and the photo-voltage satisfy linear relation. They use this relation to extract the DOS$_T$ distribution based on the TPV result[46–48]. Because of the hypothesis of exponential type distribution[46–49], their method is effective only when the TPV result is linear. The DOS$_T$ distribution extracted by their method is an exponential type distribution[46–48].

However, according to the TPV experiments reported in recent years[46–48], the majority of TPV results are nonlinear. In these cases, the method of Wang et al. is not effective to extract the DOS$_T$ distribution. In this article, we put forward a new technique for extraction of DOS$_T$ distribution based on the TPV measurement result. We give up the hypothesis of exponential type DOS$_T$ distribution[46–49] and zero-temperature approximation[46,52]. The method given in our work is based on the single hypothesis of multiple-trapping model[46,50–52]. Our method is effective for arbitrary TPV results and can be used to extract general type DOS$_T$ distribution.

Results and discussion

Establishment of theory and method. In this section, we establish the equation for the extraction of DOS$_T$ distribution based on the TPV result.

Department of Chemistry, Renmin University of China, Beijing 100872, China. email: zedonglin@ruc.edu.cn

Because of the trap states in the perovskite absorber layer, the behavior of trapping and de-trapping of carrier by the trap states determines the recombination rate, which can be described by the multiple-trapping model[46,50–52]. According to the multiple-trapping model, the relation of carrier lifetime τ_n and the free carrier lifetime τ_f satisfies[46,50–52]

$$\tau_n = (\partial n/\partial n_c)\tau_f. \tag{1}$$

Here $n = n_t + n_c$ denotes the sum of electron density in trap states n_t and electron density in conduct band n_c. Therefore, we have

$$\tau_n = (1 + \partial n_t/\partial n_c)\tau_f, \tag{2}$$

which can be rewritten as

$$\tau_n = \left(1 + \frac{\partial n_t/\partial E_{Fn}}{\partial n_c/\partial E_{Fn}}\right)\tau_f. \tag{3}$$

The density of electron in trap states satisfies[46,52]

$$n_t = \int \rho_t(E)f(E)dE. \tag{4}$$

Here $\rho_t(E)$ denotes the DOS$_T$ distribution. $f(E) = \frac{1}{exp\left(\frac{E-E_{Fn}}{k_BT}\right)+1}$ denotes the Fermi–Dirac distribution[53]. Therefore, we have

$$\frac{\partial n_t}{\partial\left(\frac{E_{Fn}}{k_BT}\right)} = \frac{\partial}{\partial\left(\frac{E_{Fn}}{k_BT}\right)}\left(\int \rho_t(E)f(E)dE\right). \tag{5}$$

According to the Fermi–Dirac distribution[53], we have

$$\frac{\partial n_t}{\partial\left(\frac{E_{Fn}}{k_BT}\right)} = \int \rho_t(E)f(E)\big(1-f(E)\big)dE. \tag{6}$$

We rewrite Eq. (6) as

$$\frac{\partial n_t}{\partial E_{Fn}} = \frac{1}{k_BT}\int \rho_t(E)f(E)\big(1-f(E)\big)dE. \tag{7}$$

The carrier density in conductor band satisfies[46,52,53]

$$n_c = N_c exp\left(\frac{E_{Fn}-E_c}{k_BT}\right). \tag{8}$$

Here N_c is the density of effective states in conduction band. E_c is the conduction band energy level position[53]. Therefore, we have

$$\partial n_c/\partial E_{Fn} = n_c/k_BT. \tag{9}$$

According to Eqs. (3), (7), and (9), we have

$$\tau_n = \left(1 + \frac{\int \rho_t(E)f(E)\big(1-f(E)\big)dE}{n_c}\right)\tau_f. \tag{10}$$

We rewrite Eq. (10) as

$$\int \rho_t(E)f(E)\big(1-f(E)\big)dE = \left(\frac{\tau_n}{\tau_f} - 1\right)n_c. \tag{11}$$

Substituting the Fermi–Dirac distribution into Eq. (11), we have

$$\int \rho_t(E)\frac{1}{exp\left(\frac{E-E_{Fn}}{k_BT}\right)+1}\left(1 - \frac{1}{exp\left(\frac{E-E_{Fn}}{k_BT}\right)+1}\right)dE = \left(\frac{\tau_n}{\tau_f} - 1\right)n_c. \tag{12}$$

We rewrite Eq. (12) as

$$\int \rho_t(E)\frac{1}{exp\left(\frac{-(E_{Fn}-E)}{k_BT}\right)+1}\left(1 - \frac{1}{exp\left(\frac{-(E_{Fn}-E)}{k_BT}\right)+1}\right)dE = \left(\frac{\tau_n}{\tau_f} - 1\right)n_c. \tag{13}$$

We define a derivation factor

Sym	Description	Value
e	Elementary charge	1.60×10^{-19} C
k_B	Boltzmann constant	1.38×10^{-23} JK^{-1}
E_c	Conduction band minimum	-4.18 eV
E_g	Band gap	1.52 eV
E_{F0}	Fermi energy level	-4.3 eV
T	Ambient temperature	300 K
N_c	Conduction band DoS	1×10^{24} m^{-3}
C_n	Electron trap coefficients	1×10^{-15} m^3 s^{-1}
N_t	Electron trap concentration	1×10^{19} m^{-3}

Table 1. Parameters used for DOS$_T$ distribution calculation[27,35].

$$g(E_{Fn} - E) = \frac{1}{exp\left(\frac{-(E_{Fn}-E)}{k_B T}\right) + 1} \left(1 - \frac{1}{exp\left(\frac{-(E_{Fn}-E)}{k_B T}\right) + 1} \right). \tag{14}$$

and rewrite Eq. (13) as

$$\int \rho_t(E) g(E_{Fn} - E) dE = \left(\frac{\tau_n}{\tau_f} - 1 \right) n_c. \tag{15}$$

According to the TPV result, the carrier lifetime is a function of photo-voltage[46–49]. Therefore, we rewrite Eq. (15) as

$$\int \rho_t(E) g(E_{Fn} - E) dE = \left(\frac{\tau_n(V_{ph})}{\tau_f} - 1 \right) n_c. \tag{16}$$

Equation (16) is the fundamental equation of our method. The right-hand side of Eq. (16) can be obtained from experimental measurement. $\tau_n(V_{ph})$ can be measured from TPV experiment. n_c can be obtained from differential charging method[5] or from SCLC under different intensity of illumination[39]. We can use absorbance spectrum, Kelvin probe (KP), ultraviolet photoemission spectroscopy (UPS), and X-ray photoelectron spectroscopy (XPS) to get conduction band energy level position E_c, valence band energy level position E_v, Fermi energy level position E_{F0} and band gap E_g[35], respectively. After getting the conductor band electron density in dark n_0 and in different intensity of illumination n_c, according to the relation $E_{Fn} = E_{F0} + k_B T ln(n_c/n_0)$[53], we obtain the electron quasi Fermi energy level E_{Fn} corresponding to the photo-voltage V_{ph} in the different intensity of illumination. The free carrier lifetime τ_f can be measured or can be calculated according to the equation $\tau_f = 1/C_n N_t$[54]. Here, N_t is the electron trap concentration. C_n denotes the capture coefficients for electrons. Since the left-hand side of Eq. (16) is the convolution integral of the DOS$_T$ distribution and the derivative factor, we can get the DOS$_T$ distribution by deconvolution. We use the numerical deconvolution function ([q,r] = deconv(u,v)) of MATLAB to solve the equation for DOS$_T$ distribution.

For intrinsic perovskite, the electron density in conductor band satisfies[53]

$$n_c = N_c exp\left(\frac{E_{Fn} - E_{cb}}{k_B T} \right) = n_0 exp\left(\frac{V_{ph} e}{2 k_B T} \right). \tag{17}$$

Here $n_0 = N_c exp\left(\frac{E_{F0} - E_{cb}}{k_B T} \right)$ is the electron density in conductor band at dark state[53].

Substituting Eq. (17) into Eq. (16), we have

$$\int \rho_t(E) g(E_{Fn} - E) dE = \left(\frac{\tau_n(V_{ph})}{\tau_f} - 1 \right) n_0 exp\left(\frac{V_{ph} e}{2 k_B T} \right). \tag{18}$$

Equation (18) is the fundamental equation for DOS$_T$ distribution extraction of intrinsic perovskite. Similarly, we obtain the DOS$_T$ distribution using numerical deconvolution function in MATLAB. The parameters used for calculation are list in Table 1[27,35].

Exponential type DOS$_T$ distribution. In this section, we explore the exponential type DOS$_T$ distribution. Wang et al.[46] find that for the exponential type DOS$_T$ distribution, the logarithm of carrier lifetime is proportional to the photo-voltage (TPV result). The proof of this relation is shown as follows.

The exponential type DOS$_T$ distribution satisfies[46–49]

$$\rho_t(E) = \frac{N_T}{E_B} exp\left(\frac{E - E_c}{E_B} \right). \tag{19}$$
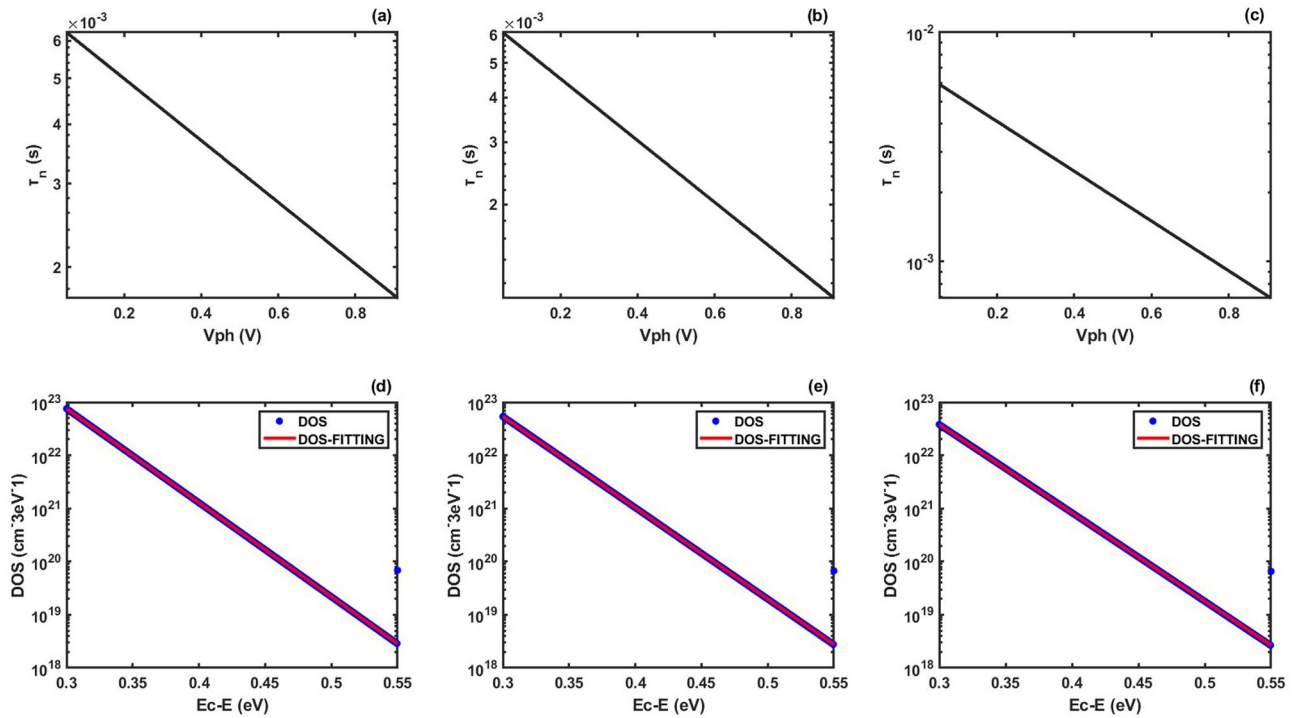
Figure 1. (**a**)–(**c**) Plots of carrier lifetime versus photo-voltage. We set $b = -5$ and a as $-1.5, -2$ and -2.5, respectively. (**d**)–(**f**) DOS_T distributions extracted from (**a**)–(**c**), respectively. The blue dots represent the extracted DOS_T distributions, the red lines represent the exponential fitting of extracted DOS_T distributions.

Here, E_B is the characteristic energy and N_T is the total density of the trapped state. Substituting formula (19) into formula (4), and taking zero-temperature approximation[46,52], we have

$$n_T = N_T \left(exp\left(\frac{E_{Fn} - E_c}{E_B} \right) - exp\left(\frac{E_v - E_c}{E_B} \right) \right). \tag{20}$$

Making the approximation of $n \approx n_T$[50], we rewrite the multiple-trapping model[46,50–52] as

$$\tau_n = (\partial n_T / \partial n_c)\tau_f, \tag{21}$$

which is equivalent to

$$\tau_n = \frac{\partial n_T / \partial V_{ph}}{\partial n_c / \partial V_{ph}} \tau_f. \tag{22}$$

The electron density in conductor band satisfies[53]

$$n_c = N_c exp\left(\frac{E_{Fn} - E_c}{k_B T} \right). \tag{23}$$

According to Eqs. (20), (22), and (23) and from the relation of $E_{Fn} = E_{Fp} + eV_{ph}$, we have

$$ln\tau_n = (e/E_B - e/k_B T)V_{ph} + lnA. \tag{24}$$

Here $A = \frac{N_T k_B T}{N_c E_B} exp\left(\frac{E_{Fp} - E_c}{E_B} - \frac{E_{Fp} - E_c}{k_B T} \right)\tau_f$.
We write Eq. (24) as linear mathematical form $ln\tau_n = aV_{ph} + b$.
Here, $a = e/E_B - e/k_B T$, $b = lnA$.
Therefore, we finish the proof of this relation. Note that for the intrinsic perovskite, Eq. (24) can be written as

$$ln\tau_n = (e/2E_B - e/2k_B T)V_{ph} + lnA. \tag{25}$$

Here $A = \frac{N_T k_B T}{N_c E_B} exp\left(\frac{E_{F0} - E_c}{E_B} - \frac{E_{F0} - E_c}{k_B T} \right)\tau_f$. We write Eq. (25) as linear form $ln\tau_n = aV_{ph} + b$. Here, $a = e/2E_B - e/2k_B T$, $b = lnA$.

Similarly, we can also prove that when TPV result is linear, the extracted DOS_T distribution is exponential type. Details of the proof are given in the supporting information. We can use this relation to extract the DOS_T distribution when the TPV result is linear. Below, this method is called analytic method.

We can use the analytic method to verify the validity of our numerical method. We use both our numerical method and the analytic method to extract the DOS_T distribution and make a comparison. In Fig. 1a–c, we set

Coefficients	Example 1	Example 2	Example 3
Chosen parameters			
a	-1.5	-2.0	-2.5
b	-5	-5	-5
Exponential fitting			
c (exponential fitting)	1.525×10^{34}	7.536×10^{33}	3.666×10^{33}
d (exponential fitting)	-2.542×10^{20}	-2.466×10^{20}	-2.388×10^{20}
R-square	1	1	1
Calculation result			
E_B(analytic method)	28.0 meV	28.8 meV	29.7 meV
E_B(our method)	24.6 meV	25.3 meV	26.1 meV
N_T(analytic method)	7.3050×10^{13} cm^{-3}	7.5158×10^{13} cm^{-3}	7.7392×10^{13} cm^{-3}
N_T(our method)	5.9992×10^{13} cm^{-3}	3.0560×10^{13} cm^{-3}	1.5352×10^{13} cm^{-3}

Table 2. Exponential fitting coefficients, distribution coefficients calculated from Fig. 2.
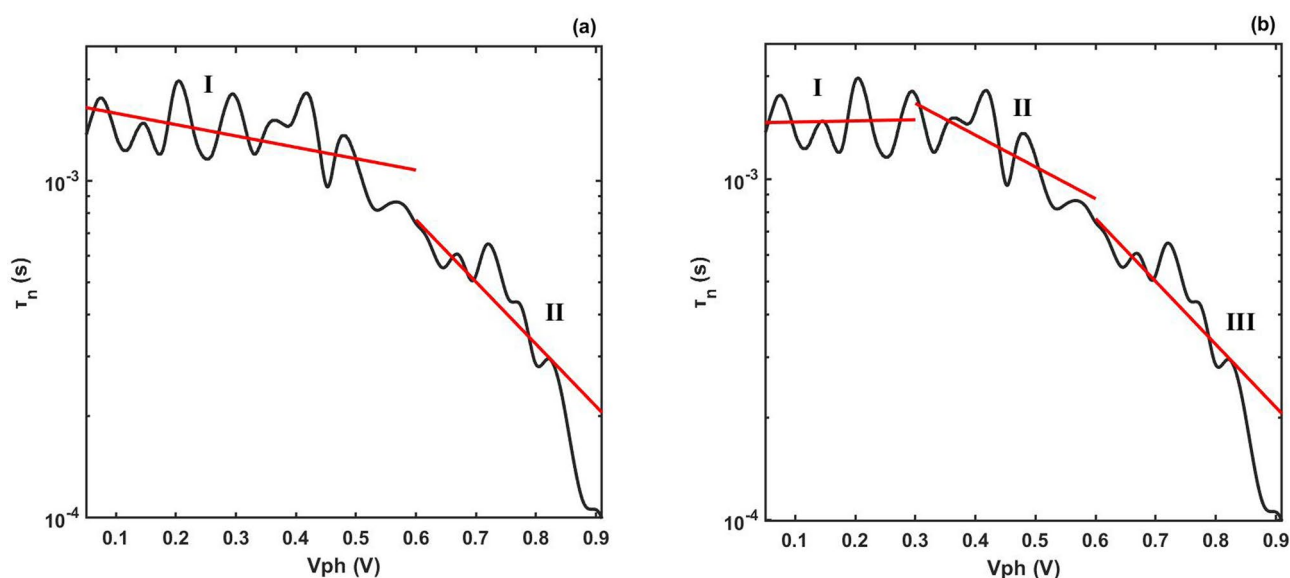

Figure 2. Plots of carrier lifetime versus photo-voltage given by TPV measurement[47]. The black lines represent the result of TPV measurement. The red lines represent linear fitting in the subintervals. (**a**) shows the linear fittings of TPV in two subintervals, respectively. (**b**) shows the linear fittings of TPV in three subintervals, respectively.

the $b = -5$ and the slope parameter a as -1.5, -2 and -2.5, respectively. Using the analytic method, we derive E_B and N_T (see Table 2). Figure 1d–f shows the extracted DOS$_T$ distributions from Fig. 1a–c using our numerical method. As expected by the analytic method, the DOS$_T$ distribution is exponential type. In order to compare with the DOS$_T$ distribution extracted by analytic method, we use the exponential fitting ($f(E) = cexp(dE)$) to calculate the E_B and N_T (see Table 2). As shown in Table 2, the E_B and N_T calculated by our numerical method are consistent with the E_B and N_T calculated by the analytic method, indicating that the numerical algorithm to do the deconvolution in our calculation is reliable. We explain the slight deviation of E_B and N_T extracted by the two methods as follows. The analytic method is established based on the three hypothesis of multiple-trapping model[46,50–52], zero-temperature approximation[46,52], and exponential type DOS$_T$ distribution[46–49]. Our numerical method is established based on the unique hypothesis of multiple-trapping model[46,50–52]. Therefore, the slight deviation of E_B and N_T extracted by the two methods is attributed to the zero-temperature approximation and the fitting error.

Non-exponential type DOS$_T$ distribution. In this section, we investigate the non-exponential type DOS$_T$ distribution. We take the TPV data in Ref.[47] as an example. As shown in Fig. 2a,b, the TPV result is non-linear. Hence, we cannot use the analytic method to extract the DOS$_T$ distribution.

To overcome this difficulty, Wang et al.[47] made a linear fitting in the subintervals of 0.05–0.6 V and 0.6–0.91 V (see Fig. 2a). They used formula (24) to get two values of E_B in these two subintervals, respectively[47]. They explained these two E_B as two types of exponential type DOS$_T$ distribution (They called them as deep trap type and shallow trap type)[47]. However, there are some difficulties in their method. (1) Equation (24) is derived from
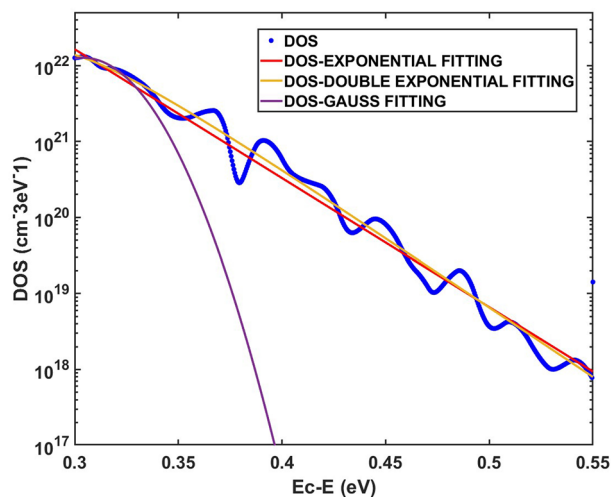
Figure 3. DOS$_T$ distribution calculated by our method given in this article. The blue dots represent the extracted DOS$_T$ distribution. The red, yellow and purple lines represent the exponential, double exponential and Gauss fittings for the extracted DOS$_T$ distribution, respectively.

Fitting type	Exponential	Double exponential	Gauss
R-square	0.9679	0.9864	0.9331

Table 3. Different type fitting for extracted DOS$_T$ distribution.

one exponential type DOS$_T$ distribution, not the two types of DOS$_T$ distribution (deep trap state type DOS$_T$ distribution and shallow trap state type DOS$_T$ distribution). We cannot derive Eq. (24) based on these two types of distribution. (2) There is no clear boundary for deep and shallow trap. So the definition of deep and shallow trap is ambiguous. (3) It is more accurate to take linear fittings in three subintervals, respectively (see Fig. 2b). According to the differential theory, we can divide the photo-voltage interval into infinite differential subintervals and use Eq. (24) to calculate the E_B in these differential subintervals, respectively. These E_B cannot be explained by the concept of deep and shallow trap.

Our method is effective for arbitrary TPV results, which can be used to extract general type DOS$_T$ distribution. Using our method, we extract the DOS$_T$ distribution (as illustrated in Fig. 3). It can be seen that the extracted DOS$_T$ distribution is not an exponential type distribution. Compared to the method given by Wang et al., our method is more accurate and it can give the fine structure of DOS$_T$ distribution.

We make the exponential, double exponential and Gauss fittings for the extracted DOS$_T$ distribution, respectively (see Fig. 3). The R-square (Coefficient of determination) of these fittings are given in Table 3. It can be see that the R-square of double exponential fitting is larger than the exponential fitting and Gauss fitting, indicating that the DOS$_T$ distribution is more consistent with the double exponential type distribution than with the exponential type distribution. Therefore, when the TPV result is non-linear, the extracted DOS$_T$ distribution is non-exponential type.

Calculation example. In this section, we give some examples of DOS$_T$ distribution extraction using our method. We take the TPV data in Ref.[47] as an example. Figure 4a–c shows the TPV results for meso-structured perovskite solar cells with large, middle and small size of perovskite grain, respectively. Using our method, we extract the DOS$_T$ distributions from Fig. 4a–c, respectively, (as shown in Fig. 4d–f).

For comparing, we plot the extracted DOS$_T$ distributions in Fig. 5. Using the formula $T_{total} = \int \rho_t(E)dE$, we calculate the total amount of trap states for three solar cells. We derived $T_{total} = 5.4431 \times 10^{20}$ cm^{-3} (large size), $T_{total} = 5.9096 \times 10^{20}$ cm^{-3} (middle size) and $T_{total} = 4.5628 \times 10^{20}$ cm^{-3} (small size). It can be seen that the solar cell with small size of perovskite grain has the least amount of trap states. This result could give a guidance for preparing perovskite solar cells with less trap states.

Comparison to SCLC method. SCLC measurement gives the relation of current density and voltage at different temperatures ($j = j(U, T)$). For SCLC method, we extract the DOS$_T$ distribution adopting the equations listed as follows[35–40]
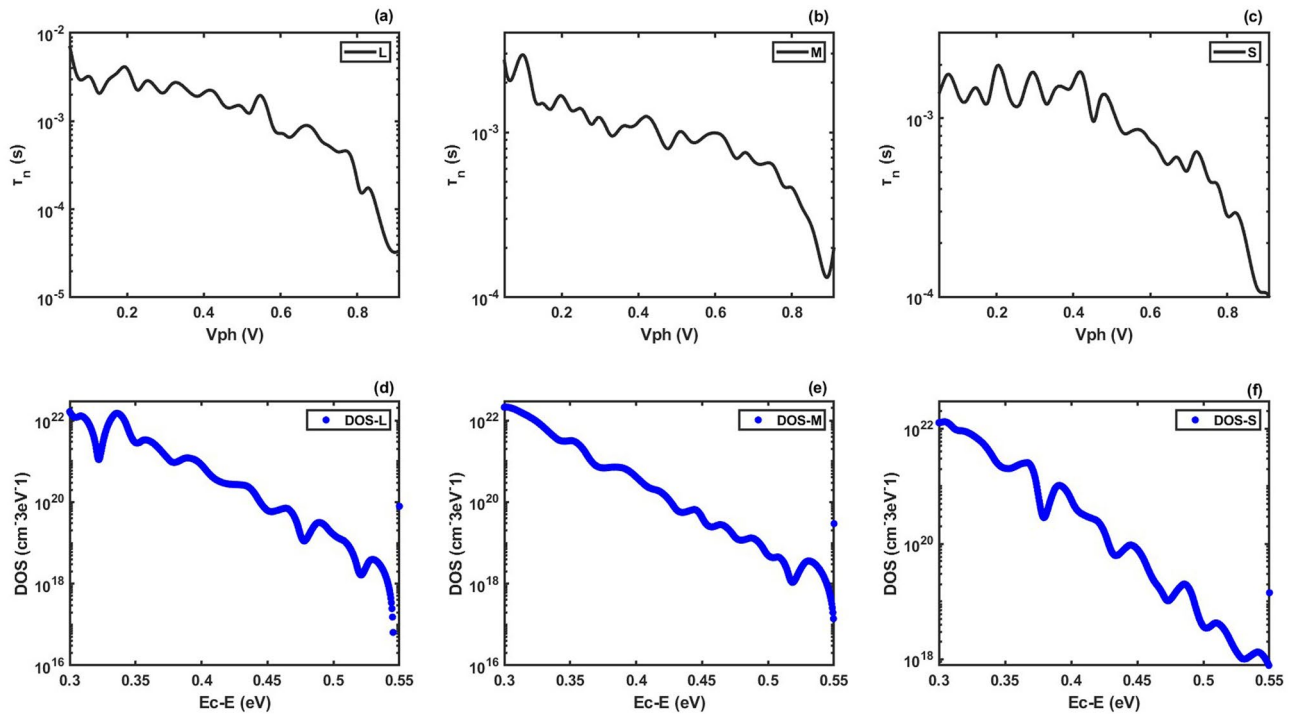
$$E_a = -dlnj/d(k_BT)^{-1},$$ (26)

Figure 4. (**a**)–(**c**) TPV results for meso-structured perovskite solar cells with large, middle and small size of perovskite grain[47]. (**d**)–(**f**) DOS_T distributions extracted by our method from (**a**)–(**c**), respectively.
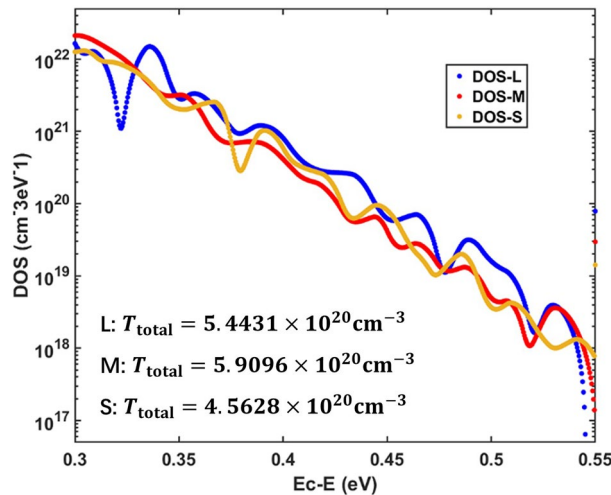

Figure 5. DOS_T distributions for meso-structured perovskite solar cells with large, middle and small size of perovskite grain extracted by our method given in this paper.

$$m = d(lnj)/d(lnU), \tag{27}$$

$$B = -[dm/d(lnU)]/[m(m-1)(2m-1)], \tag{28}$$

$$C = \left(B(2m-1) + B^2(3m-2) + d(ln(1+B))/d(lnU)\right)/(1+B(m-1)), \tag{29}$$

$$\int \rho_t(E)f(E)\left(1-f(E)\right)dE = \frac{1}{k_B T}\frac{\varepsilon U}{eL^2}\frac{2m-1}{m^2}(1+C). \tag{30}$$

Here j denotes the current density. U denotes the voltage. E_a is the activation energy. m, B, C are the parameters for calculation. L is the thickness of perovskite absorber layer. e is the elementary charge. ε is the dielectric
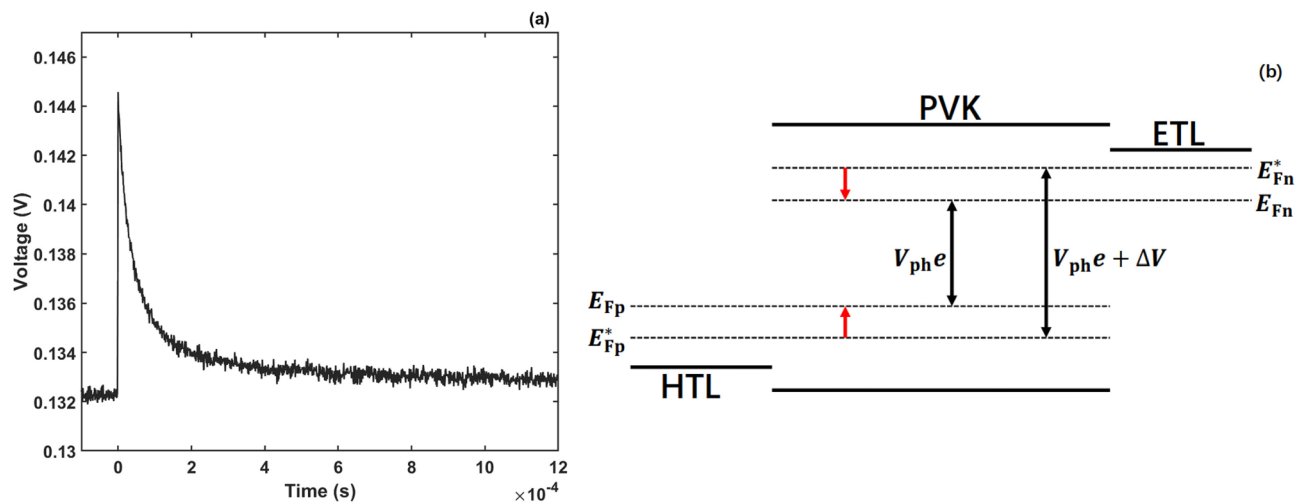
Figure 6. (**a**) Result of TPV measurement. (**b**) Mechanism of TPV experiment.

constant of perovskite absorber layer. Based on the SCLC measurement result, we need to calculate E_a, m, B, C and finally use Eq. (30) to extract the DOS_T by deconvolution[35–40]. The calculations of E_a, m, B, C are complicated. For our method, we only need to use formula (18) to extract the DOS_T distribution by deconvolution. Therefore, our method takes less computation.

Conclusion

In conclusion, this article presents a new technique for DOS_T distribution extraction based on the TPV measurement result. The approach given in this paper is effective for extraction of general type DOS_T distribution. We prove that when the TPV result is linear, the DOS_T distribution is exponential type and vice versa. Our method needs less computation than the SCLC method. The obtained results provide a guidance for preparing perovskite solar cells with less trap states.

Methods

The transient photo-voltage measurement is an effective technique for the study of carrier recombination[3,46–49]. Figure 6a shows the typical TPV measurement result. Figure 6b shows the mechanism of TPV experiment. Photo-voltaic device is held under open circuit. At the start of the TPV experiment, we use a steady-state bias light to illuminate the device until the equilibrium between generation and recombination is established. The steady-state bias light produces a bias photo-voltage V_{ph}. As a result, the Fermi energy level E_{F0} changes to electron quasi Fermi energy level E_{Fn} and hole quasi Fermi energy level E_{Fp}. Thereafter, we apply an additional small light pulse to the device. With the perturbation of small light pulse, the photo-voltage increases to $V_{ph} + \Delta V$. The electron quasi Fermi energy level E_{Fn} shifts to E_{Fn}^*, and the hole quasi Fermi energy level E_{Fp} to E_{Fp}^*. After switching off the small light pulse source, due to carrier recombination, the photo-voltage decays exponentially until it reaches the bias value V_{ph}. The electron quasi Fermi energy level comes back to E_{Fn} from E_{Fn}^* and the hole quasi Fermi energy level comes back to E_{Fp} from E_{Fp}^*. The carrier lifetime τ_n is defined as the time taken for the photo-voltage to decay from $V_{ph} + \Delta V$ to $V_{ph} + \Delta V/e$. Here, e is the natural constant. By tuning the intensity of steady-state bias light I, we get the relation between the photo-voltage V_{ph} and carrier lifetime τ_n, which is written as $\tau_n = \tau_n(V_{ph})$ (TPV result)[46–49].

References

1. Khan, M. T., Salado, M., Almohammedi, A., Kazim, S. & Ahmad, S. Elucidating the impact of charge selective contact in halide perovskite through impedance spectroscopy. *Adv. Mater. Interfaces* **6**, 1901193 (2019).
2. Juška, G., Arlauskas, K., Viliūnas, M. & Kočka, J. Extraction current transients: new method of study of charge transport in micro-crystalline silicon. *Phys. Rev. Lett.* **84**, 4946–4949 (2000).
3. Mäckel, H. & MacKenzie, R. C. I. Determination of charge-carrier mobility in disordered thin-film solar cells as a function of current density. *Phys. Rev. Appl.* **9**, 034020 (2018).
4. Senocrate, A. *et al.* The nature of ion conduction in methylammonium lead iodide: a multimethod approach. *Angew. Chem. Int. Ed.* **56**, 7755–7759 (2017).
5. Yang, T., Gregori, G., Pellet, N., Grätzel, M. & Maier, J. The significance of ion conduction in a hybrid organic-inorganic lead-iodide-based perovskite photosensitizer. *Angew. Chem. Int. Ed.* **54**, 7905–7910 (2015).
6. Yuan, Y. & Huang, J. Ion migration in organometal trihalide perovskite and its impact on photovoltaic efficiency and stability. *Acc. Chem. Res.* **49**, 286–293 (2016).
7. Eames, C. *et al.* Ionic transport in hybrid lead iodide perovskite solar cells. *Nat. Commun.* **6**, 7497 (2015).
8. Levine, I. *et al.* Interface-dependent ion migration/accumulation controls hysteresis in mapbi3 solar cells. *J. Phys. Chem. C* **120**, 16399–16411 (2016).

9. Kearney, K. *et al.* Computational analysis of the interplay between deep level traps and perovskite solar cell efficiency. *J. Am. Chem. Soc.* **140**, 15655–15660 (2018).
10. Bai, Y. *et al.* Oligomeric silica-wrapped perovskites enable synchronous defect passivation and grain stabilization for efficient and stable perovskite photovoltaics. *ACS Energy Lett.* **4**, 1231–1240 (2019).
11. Li, X. *et al.* Furrowed hole-transport layer using argon plasma in an inverted perovskite solar cell. *New J. Chem.* **43**, 14625 (2019).
12. Cai, F. *et al.* Ionic additive engineering toward high-efficiency perovskite solar cells with reduced grain boundaries and trap density. *Adv. Funct. Mater.* **28**, 1801985 (2018).
13. Shi, D. *et al.* Low trap-state density and long carrier diffusion in organolead trihalide perovskite single crystals. *Science* **347**, 519–522 (2015).
14. Calado, P. *et al.* Identifying dominant recombination mechanisms in perovskite solar cells by measuring the transient ideality factor. *Phys. Rev. Appl.* **11**, 044005 (2019).
15. Kirchartz, T., Pieters, B. E., Kirkpatrick, J., Rau, U. & Nelson, J. Recombination via tail states in polythiophene: fullerene solar cells. *Phys. Rev. B* **83**, 115209 (2011).
16. Ostroverkhova, O. Organic optoelectronic materials: mechanisms and applications. *Chem. Rev.* **116**, 13279–13412 (2016).
17. Sherkar, T. S., Momblona, C., Gil-Escrig, L., Bolink, H. J. & Koster, L. J. A. Improving perovskite solar cells: insights from a validated device model. *Adv. Energy Mater.* **7**, 1602432 (2017).
18. Ren, X., Wang, Z., Sha, W. E. I. & Choy, W. C. H. Exploring the way to approach the efficiency limit of perovskite solar cells by drift-diffusion model. *ACS Photonics* **4**, 934–942 (2017).
19. Shao, Y., Xiao, Z., Bi, C., Yuan, Y. & Huang, J. Origin and elimination of photocurrent hysteresis by fullerene passivation in ch3nh3pbi3 planar heterojunction solar cells. *Nat. Commun.* **5**, 5784 (2014).
20. van Reenen, S., Kemerink, M. & Snaith, H. J. Modeling anomalous hysteresis in perovskite solar cells. *J. Phys. Chem. Lett.* **6**, 3808–3814 (2015).
21. Richardson, G. *et al.* Can slow-moving ions explain hysteresis in the current voltage curves of perovskite solar cells. *Energy Environ. Sci.* **9**, 1476–1485 (2016).
22. Calado, P. *et al.* Evidence for ion migration in hybrid perovskite solar cells with minimal hysteresis. *Nat. Commun.* **7**, 13831 (2016).
23. Courtier, N. E., Cave, J. M., Foster, J. M., Walker, A. B. & Richardson, G. How transport layer properties affect perovskite solar cell performance: insights from a couples charge transport/ion migration model. *Energy Environ. Sci.* **12**, 396–409a (2019).
24. Ran, C., Xu, J., Gao, W., Huang, C. & Dou, S. Defects in metal triiodide perovskite materials towards high-performance solar cells: origin, impact, characterization, and engineering. *Chem. Soc. Rev.* **47**, 4581–4610 (2018).
25. Luo, D., Su, R., Zhang, W., Gong, Q. & Zhu, R. Minimizing non-radiative recombination losses in perovskite solar cells. *Nat. Rev. Mater.* **5**, 44–60 (2020).
26. Lakhwani, G., Rao, A. & Friend, R. H. Bimolecular recombination in organic photovoltaics. *Annu. Rev. Phys. Chem.* **65**, 557–581 (2014).
27. Sherkar, T. S. *et al.* Recombination in perovskite solar cells: significance of grain boundaries, interface traps, and defect ions. *ACS Energy Lett.* **2**, 1214–1222 (2017).
28. Sandberg, O. J., Sundqvist, A., Nyman, M. & Österbacka, R. Relating charge transport, contact properties, and recombination to open-circuit voltage in sandwich-type thin-film solar cells. *Phys. Rev. Appl.* **5**, 044005 (2016).
29. Azzouzi, M., Kirchartz, T. & Nelson, J. Factors controlling open-circuit voltage losses in organic solar cells. *Trends Chem.* **1**, 50–62 (2019).
30. Tress, W., Leo, K. & Riede, M. Dominating recombination mechanisms in organic solar cells based on znpc and c60. *Appl. Phys. Lett.* **102**, 163901 (2013).
31. Zheng, X. *et al.* Defect passivation in hybrid perovskite solar cells using quaternary ammonium halide anions and cations. *Nat. Energy* **2**, 17102 (2017).
32. Shiiba, H., Nakayama, M., Kasuga, T., Grimes, R. W. & Kilner, J. A. Calculation of arrangement of oxygen ions and vacancies in double perovskite gdbaco2o5+δ by first-principles dft with Monte Carlo simulations. *Phys. Chem. Chem. Phys.* **15**, 10494–10499 (2013).
33. Saffari, M., Mohebpour, M. A., Soleimani, H. R. & Tagani, M. B. Dft analysis and fdtd simulation of ch3nh3pbi3-*x*cl*x* mixed halide perovskite solar cells: role of halide mixing and light trapping technique. *J. Phys. D* **50**, 415501 (2017).
34. Kim, J., Yun, A. J., Gil, B., Lee, Y. & Park, B. Triamine-based aromatic cation as a novel stabilizer for efficient perovskite solar cells. *Adv. Funct. Mater.* **29**, 1905190 (2019).
35. Adinolfi, V. *et al.* The in-gap electronic state spectrum of methylammonium lead iodide single-crystal perovskites. *Adv. Mater.* **28**, 3406–3410 (2016).
36. Schauer, F., Novotny, R. & Nešpůrek, S. Space-charge-limited-current spectroscopy: possibilities and limitations. *J. Appl. Phys.* **81**, 1244–1249 (1997).
37. Dacuña, J. & Salleo, A. Modeling space-charge-limited currents in organic semiconductors: extracting trap density and mobility. *Phys. Rev. B* **84**, 195209 (2011).
38. Schauer, F., Nešpůrek, S. & Valerián, H. Temperature dependent space-charge-limited currents in amorphous and disordered semiconductors. *J. Appl. Phys.* **80**, 880–888 (1996).
39. Pospisil, J. *et al.* Density of bulk trap states of hybrid lead halide perovskite single crystals: temperature modulated space-charge-limited-currents. *Sci. Rep.* **9**, 3332 (2019).
40. Krellner, C. *et al.* Density of bulk trap states in organic semiconductor crystals: discrete levels induced by oxygen in rebrene. *Phys. Rev. B* **75**, 245115 (2007).
41. Walter, T., Herberholz, R., Müller, C. & Schock, H. W. Determination of defect distributions from admittance measurements and application to cu(in, ga)se2 based heterojunctions. *J. Appl. Phys.* **80**, 4411–4420 (1996).
42. Duan, H. *et al.* The identification and characterization of defect states in hybrid organic-inorganic perovskite photovoltaics. *Phys. Chem. Chem. Phys.* **17**, 112–116 (2015).
43. von Hauff, E. Impedance spectroscopy for emerging photovoltaics. *J. Phys. Chem. C* **123**, 11329–11346 (2019).
44. Lee, B. *et al.* Aminosilane-modified cugao2 nanoparticles incorporated with cuscn as a hole-transport layer for efficient and stable perovskite solar cells. *Adv. Mater. Interfaces* **6**, 1901372 (2019).
45. Hwang, T. *et al.* Electronic traps and their correlations to perovskite solar cell performance via compositional and thermal annealing controls. *ACS Appl. Mater. Interfaces* **11**, 6907–6917 (2019).
46. Wang, Y. *et al.* Correlation between energy and spatial distribution of intragap trap states in the tio2 photoanode of dye-sensitized solar cells. *Chem. Phys. Chem.* **16**, 2253–2259 (2015).
47. Wang, H. *et al.* Mechanism of biphasic charge recombination and accumulation in tio2 mesoporous structured perovskite solar cells. *Phys. Chem. Chem. Phys.* **18**, 12128–12134 (2016).
48. Zhao, J. *et al.* Charge carrier recombination dynamics in a bi-cationic perovskite solar cell. *Phys. Chem. Chem. Phys.* **21**, 5409–5415 (2019).
49. Wang, H. *et al.* Adverse effects of excess residual pbi2 on photovoltaic performance, charge separation, and trap-state properties in mesoporous structured perovskite solar cells. *Chem. Eur. J.* **23**, 3986–3992 (2017).
50. Bisquert, J. & Vikhrenko, V. S. Interpretation of the time constants measured by kinetic techniques in nanostructured semiconductor electrodes and dye-sensitized solar cells. *J. Phys. Chem. B* **108**, 2313–2322 (2004).

51. Bisquert, J., Fabregat-Santiago, F., Mora-Seró, I., Garcia-Belmonte, G. & Giménez, S. Electron lifetime in dye-sensitized solar cells: theory and interpretation of measurements. *J. Phys. Chem. C* **113**, 17278–17290 (2009).
52. Wang, H. *et al.* Multiple-trapping model for the charge recombination dynamics in mesoporous-structured perovskite solar cells. *Chem. Sus. Chem.* **10**, 4872–4878 (2017).
53. Nelson, J. *The Physics of Solar Cells* (Imperial College Press, London, 2003).
54. Street, R. A. Trapping parameters of dangling bonds in hydrogenated amorphous silicon. *Appl. Phys. Lett.* **41**, 1060–1062 (1982).

Competing interests
The author declares no competing interests.

Additional information
Supplementary information is available for this paper at https://doi.org/10.1038/s41598-020-69914-y.

Correspondence and requests for materials should be addressed to Z.L.

Reprints and permissions information is available at www.nature.com/reprints.

Publisher's note Springer Nature remains neutral with regard to jurisdictional claims in published maps and institutional affiliations.